Supplemental Document

Optics EXPRESS

Statistical optics modeling of dark-field scattering in X-ray grating interferometers: Part 2. Simulation: supplement

JEFFREY P. WILDE[1,*] AND LAMBERTUS HESSELINK[1,2]

[1]*E. L. Ginzton Laboratory, Stanford University, Stanford, CA 94305, USA*
[2]*Department of Electrical Engineering, Stanford University, Stanford, CA 94305, USA*
[*]*jpwilde@stanford.edu*

Supplement DOI: https://doi.org/10.6084/m9.figshare.16988086

Parent Article DOI: https://doi.org/10.1364/OE.447798

Statistical optics modeling of dark-field scattering in X-ray grating interferometers: supplemental document

In this supplement, we provide details associated with two separate topics.

The first topic relates to the convolutional blurring model for the dark-field effect. We summarize the model as it has been applied in the literature, address some of its deficiencies, and then propose a modified version that aligns with the statistical optics approach. The final result, as stated in Eq. S25, is actually quite straightforward. It states that the Talbot fringe is comprised of two portions, namely specular and scattered components with relative weights dictated by the variance of the phase perturbation. The scattered fringe component is given by a convolution of an *effective* scattered spot function with the nominal Talbot fringe (in the absence of scattering) which reduces the visibility of this component.

The second section provides a derivation of the autocorrelation function for the refractive index distribution associated with a random ensemble of hard microspheres. This 3D autocorrelation function is used in the statistical optics model to evaluate the 2D autocorrelation function of the scattered radiation field, which in turn allows us to find the detected visibility of the Talbot fringe.

1. CONVOLUTIONAL BLURRING MODEL

Convolutional blurring is a phenomenological model in which a small, spatially localized region of the object generates a cone of small-angle scattered radiation, typically taken to have a Gaussian distribution in angle space. Upon reaching the detection plane, this scattered radiation forms a spot with a Gaussian intensity profile that can be considered a type of scattering point-spread function. The width of this Gaussian impulse response can range from much less than the fringe period to much greater, depending on the size of the scattering particles. When the spot width is on the order of or greater than the fringe period, a convolution of the scattering impulse response with the nominal Talbot fringe pattern (formed in the absence of scattering) yields a blurred version of the fringe with reduced visibility. In the literature, various investigators have utilized this model [1–4]. The scattering properties of the object are in general spatially varying, so an object can be viewed as a space-variant system comprised of localized isoplanatic regions, each having its own scattering impulse response.

To analyze this model as previously implemented in the literature, we begin with a Gaussian scatter blur spot intensity given by

$$g(x,y) = \frac{1}{4\pi r_0^2} e^{-\left(x^2+y^2\right)/\,r_0^2}. \tag{S1}$$

We also choose the nominal phase of the reference Talbot fringe (without scattering) such that the fringe intensity can be expressed as a Fourier sine series,

$$I_{T0}(x,y) = I_0 + \sum_{n=1}^{N} b_n \sin(2\pi n x/p_2). \tag{S2}$$

The convolution of these two functions is readily carried out in the Fourier domain as,

$$I_T(x,y) = g(x,y) * I_{T0}(x,y) = \mathcal{F}^{-1}\left\{G(\nu_x,\nu_y)\mathscr{I}_{T0}(\nu_x,\nu_y)\right\}, \tag{S3}$$

where the transforms of $g(x,y)$ and $I_{T0}(x,y)$ are, respectively,

$$G(\nu_x,\nu_y) = \exp\left[-(\pi r_0)^2\left(\nu_x^2+\nu_y^2\right)\right], \tag{S4}$$

and

$$\mathscr{I}_{T0}(\nu_x,\nu_y) = I_0\delta(\nu_x,\nu_y) + \frac{i}{2}\sum_{n=1}^{N} b_n\left[\delta(\nu_x + n/p_2,\nu_y) - \delta(\nu_x - n/p_2,\nu_y)\right]. \tag{S5}$$

Explicitly writing the inverse transform and using the sifting property of the delta functions in $\mathscr{I}_{T0}(\nu_x,\nu_y)$ leads to

$$\begin{aligned} I_T(x,y) = g(x,y) * I_{T0}(x,y) &= \iint_{-\infty}^{\infty} G(\nu_x)\mathscr{I}_{T0}(\nu_x)e^{i2\pi(\nu_x x+\nu_y y)}d\nu_x d\nu_y \\ &= I_0 + \frac{i}{2}\sum_{n=1}^{N} b_n e^{-(\pi r_0 n/p_2)^2}\left(e^{-i2\pi nx/p_2} - e^{i2\pi nx/p_2}\right) \\ &= I_0 + \sum_{n=1}^{N} b_n e^{-(\pi r_0 n/p_2)^2}\sin(2\pi nx/p_2). \end{aligned} \tag{S6}$$

If we let

$$\xi_n = \exp\left[-(\pi r_0 n/p_2)^2\right], \tag{S7}$$

then the Talbot fringe in the presence of scattering becomes

$$I_T(x,y) = I_0 + \sum_{n=1}^{N}\xi_n b_n \sin(2\pi nx/p_2). \tag{S8}$$

This result is similar to our previous finding of Eq. 12 based on coherence considerations, so at first glance we are tempted to view ξ_n as analogous to a field coherence function.

While this approach is attractive for its apparent simplicity, it is problematic for a few key reasons. First, for a monochromatic source, we saw in Sec. 5 that the scattered radiation creates a speckled version of the Talbot fringe, not a locally smooth "blurred" version, so the physical picture is not strictly correct. However, this need not stop us from applying the model, or some variant of it, if it yields a potentially useful result. Second, we know from Sec. 4.4 (see Eq. 49) that the field coherence function, or normalized field autocorrelation function, evaluated at the detection plane is generally of the form (assuming a thin medium with $\rho_q = 1$),

$$\gamma_q = \mu_d(\Delta x_q) = \exp\left[-\sigma_\phi^2\left(1 - c_\phi\left(\frac{z_s}{L+d}\Delta x_q\right)\right)\right]. \tag{S9}$$

Even though the normalized autocovariance function of the scattering object's phase profile, c_ϕ, may be well approximated by a Gaussian (particularly for a low concentration of scattering particles when $f << 1$), the field coherence function will in general not be Gaussian in contrast to Eq. S7 for ξ_n. Third, if the field coherence function were purely Gaussian, decaying to zero with increasing n as suggested by Eq. S7, then there would be no specular component.[1] However, as we saw in Sec. 4.5.1, lack of a specular component means we are only considering the regime in which $\sigma_\phi \geq 2.0$. Lastly, the phenomolgical blurring model suggests that for a given scattering object, the blur spot size r_0 should increase as the distance between the object and the detection plane increases. This in turn means the visibility should only decrease as the object moves farther away from the detection plane. However, this behavior is not consistent with our previous findings (see Fig. 9), where the visibility goes up if the object is placed in front of G_1 and is moved farther away from the detection plane, although some previous work has addressed this problem [3, 4]. Clearly, though, some modifications are in order if we would like to have a blurring model that is consistent with the more rigorous statistical optics model. In the remainder of this section we develop a new version of the convolutional blurring model that overcomes the aforementioned deficiencies.

We begin by modifying the statistical optics model to put it into a slightly different form that is more amenable for comparison to the new convolutional blurring formulation. For this purpose we assume $c_\phi(\Delta\alpha)$ is Gaussian, as was previously done in Sec. 4.5.1 (Eq. 57),

$$c_\phi(\Delta\alpha) = \exp\left[-(\Delta\alpha/R)^2\right], \tag{S10}$$

[1] If a specular component of a monochromatic beam were present, then this component would always remain spatially correlated with itself for arbitrary lateral separation, meaning the field coherence function would have a non-zero asymptote for large separations (see [5], Sec. 5.4.2). The converse implies that a beam with an ensemble-average coherence function that decays to zero must have no specular component.

where R is a correlation radius related to the spatial frequency content of the scattering object's phase profile. Setting $\Delta\alpha = \Delta x_q z_s/(L+d)$ and using Eq. 50 for Δx_q, the expression for the coherence coefficients (Eq. S9) becomes

$$\gamma_q = \exp\left[-\sigma_\phi^2\left(1-e^{-(q/q_0)^2}\right)\right], \tag{S11}$$

where

$$q_0 = \frac{p_1 R}{\lambda}\cdot\begin{cases}\left(\dfrac{L+d}{z_s}\right)\left(\dfrac{1}{d}\right) & 0<z_s\le L\\ \left(\dfrac{L+d}{z_s}\right)\left(\dfrac{1}{L+d-z_s}\right) & L<z_s<L+d.\end{cases} \tag{S12}$$

We can now attempt to create a version of the convolutional blurring model with coherence coefficients that better match this result.

To construct such a modified convolutional blurring model, we start by making a small change to the Gaussian blur spot definition of Eq. S1 to account for the type of G_1 phase grating by letting $r_0 \to r_0/\eta$:

$$\hat{g}(x,y) = \frac{1}{4\pi\eta^2 r_0^2} e^{-\eta^2\left(x^2+y^2\right)/r_0^2}, \tag{S13}$$

where $\eta = 1$ for a $\pi/2$-phase G_1 and $\eta = 2$ for a π-phase G_1. The same change is also made to the exponential of Eq. S7,

$$\widehat{\xi}_n = \exp\left[-\left(\pi r_0 n/\eta p_2\right)^2\right] = \exp\left[-\left(n/n_0\right)^2\right], \tag{S14}$$

with $n_0 = \eta p_2/\pi r_0$. Next, we adopt a revised expression for the coherence coefficients that includes a specular component plus the Gaussian coherence function ξ_n weighted by the fraction of scattered power as follows:

$$\zeta_n \triangleq \underbrace{e^{-\sigma_\phi^2}}_{\substack{\text{specular}\\ \text{fraction}}} + \underbrace{\left(1-e^{-\sigma_\phi^2}\right)}_{\substack{\text{scattered}\\ \text{fraction}}}\widehat{\xi}_n. \tag{S15}$$

A third change comes from assuming the radial blur spot size is generated by a scattered cone of radiation (with a cone half-angle of θ_s) propagating over an *effective distance*, d_{eff}:

$$r_0 = \theta_s d_{\text{eff}}, \tag{S16}$$

where d_{eff} depends on whether the scattering object is located before or after G_1,

$$d_{\text{eff}} = \begin{cases} z_s d/L & 0<z_s\le L\\ L+d-z_s & L<z_s<L+d.\end{cases} \tag{S17}$$

Note that d_{eff} varies with z_s in the same way that the differential phase contrast sensitivity does [6]; namely, it starts at zero when the object is next to G_0 ($z_s = 0$), rises linearly to equal d when the object is next to G_1 ($z_s = L$), then decreases linearly to zero as the object moves toward the detection plane. Thus, the parameter n_0 in Eq. S14 becomes,

$$n_0 = \frac{\eta p_2}{\pi r_0} = \frac{\eta p_2}{\pi\theta_s d_{\text{eff}}} = \frac{p_1}{\pi\theta_s d_{\text{eff}}}\left(1+\frac{d}{L}\right). \tag{S18}$$

Here we used a known relation for the period of G_2, namely $p_2 = (p_1/\eta)(1+d/L)$ [7]. Lastly, the scattering cone half-angle, θ_s, depends on the ensemble-average coherence area of the radiation field leaving the scatterer. If the field coherence area is denoted as A_μ, then the solid angle of the scattered radiation is given by $\Omega_s = \lambda^2/A_\mu$ (see [8], Eq. 6.12). The solid angle is related to the cone half-angle via $\Omega_s = \pi\theta_s^2$, so

$$\theta_s = \frac{\lambda}{\sqrt{\pi A_\mu}}. \tag{S19}$$

For a random phase object, Goodman has derived the following function that relates the coherence area of the scattered field to the correlation area, πR^2, of the phase profile ([5], Eq. 5.64),

$$\chi(\sigma_\phi) = \frac{A_\mu(\sigma_\phi)}{\pi R^2} = \frac{e^{-\sigma_\phi^2}}{1-e^{-\sigma_\phi^2}}\left[\text{Ei}\left(\sigma_\phi^2\right) - \mathcal{E} - \ln\left(\sigma_\phi^2\right)\right], \tag{S20}$$

where $\mathrm{Ei}(x)$ represents the exponential integral, and $\mathcal{E} = 0.577216$ is Euler's constant ([9], p. 15, Eq. 1.2.5). Here the phase correlation radius, R, is precisely the same as that used in the statistical optics model (Eq. S10). Roughly speaking, R is the characteristic particle size of the scattering object. The scattering angle can now be written as,

$$\theta_s(\sigma_\phi) = \frac{\lambda}{\pi R\sqrt{\chi(\sigma_\phi)}}. \tag{S21}$$

Inserting this expression for θ_s, along with Eq. S17 for d_{eff}, into Eq. S18, we have

$$n_0 = \frac{p_1 R\sqrt{\chi(\sigma_\phi)}}{\lambda} \cdot \begin{cases} \left(\dfrac{L+d}{z_s}\right)\left(\dfrac{1}{d}\right) & 0 < z_s \leq L \\ \left(\dfrac{L+d}{L}\right)\left(\dfrac{1}{L+d-z_s}\right) & L < z_s < L+d. \end{cases} \tag{S22}$$

Comparison with Eq. S12 for q_0 shows $n_0 \simeq q_0\sqrt{\chi(\sigma_\phi)}$, with equality occurring when the scattering object is placed adjacent to G_1 (i.e., $z_s = L$).

This completes our modified version of the convolutional blurring model. To summarize, the Talbot fringe in the presence of a thin scattering object (with $\rho_q = 1$) is given by

$$I_T(x,y) = I_0 + \sum_{n=1}^{N} \zeta_n b_n \sin(2\pi n x/p_2), \tag{S23}$$

with the following expression for the coherence coefficients:

$$\zeta_n = e^{-\sigma_\phi^2} + (1 - e^{-\sigma_\phi^2})e^{-(n/n_0)^2}. \tag{S24}$$

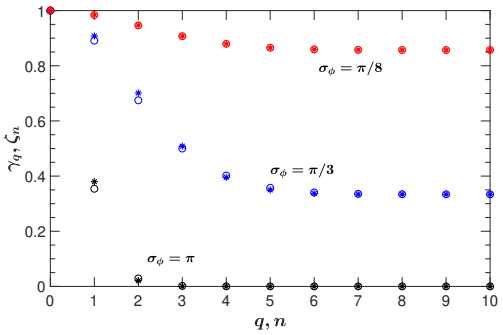

Fig. S1. Comparison of γ_q coherence coefficients (statistical optics model, Eq. S12) plotted with circles, and ζ_n coefficients (modified convolutional blurring model, Eq.S24) plotted with asterisks. For these plots $q_0 = 3$ and the scattering object is located adjacent to G_1 (i.e., $z_s = L$) so $n_0 = q_0\sqrt{\chi(\sigma_\phi)}$.

In terms of a convolution with the modified blur spot $\hat{g}(x,y)$, Eq. S23 can be rewritten as

$$I_T(x,y) = \underbrace{e^{-\sigma_\phi^2} I_{T0}(x,y)}_{\substack{\text{specular} \\ \text{portion}}} + \underbrace{(1 - e^{-\sigma_\phi^2})\, \hat{g}(x,y) * I_{T0}(x,y)}_{\substack{\text{scattered} \\ \text{portion}}}, \tag{S25}$$

with the blur spot size, r_0, given by Eq. S16 (in combination with Eq. S17 and Eq. S21). This formulation is best suited for scattering objects having a low concentration of scattering particles (i.e., $f \lesssim 0.1$) that are well-approximated by a Gaussian phase correlation function. The value of n_0, as given by Eq. S22, determines how quickly the amplitudes of the various terms in the Fourier sine expansion are reduced by loss of ensemble-average coherence as a consequence of scattering. The visibility of the Talbot fringe is dominated by the b_1 term, while the higher-order

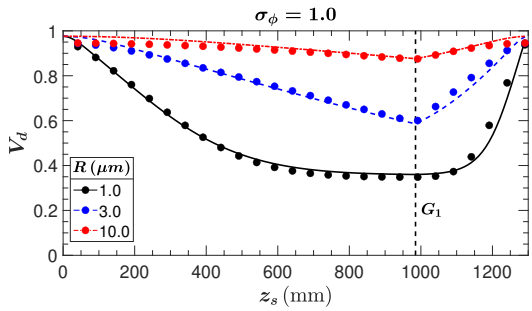

Fig. S2. Plots of $V_d(z_s)$ for a dilute suspension of monodispere microspheres, represented by a random Gaussian phase screen. The graph lines are from the previous statistical optics analysis (Fig. 9b), while the solid circles are for our modified convolutional blurring model.

coefficients affect the cross-sectional shape of the fringe. Ultimately, the detected visibility signal derives from a convolution of the G_2 analyzer grating transmission function with $I_T(x, y)$.

In Figure S1 we show example plots of γ_q and ζ_n for various values of σ_ϕ. While these two functions are not identical, their correspondence is very close to one another. Indeed, if we use the statistical optics model but replace γ_q with ζ_n (and use n in place of q) we obtain almost the same results. For example, Figure S2 shows the detected visibility versus scattering object location for the two models.

2. AUTOCORRELATION FUNCTION OF A RANDOM DISTRIBUTION OF HARD SPHERICAL PARTICLES

In this section, we provide a derivation of the autocorrelation function for a random distribution of impenetrable "hard" microspheres following the approach described by Torquato and Stell [10]. An alternate approach as been recently published by Lee *et al.* for the analysis of photonic glasses [11]. We restrict our discussion to the case of a monodisperse ensemble in which all of the microspheres have the same diameter. This is an interesting case not only because it demonstrates, in a theoretically tractable fashion, the key features characteristic in extending the analysis from a single sphere to multiple spherical scatterers, but it is one that can be readily implemented experimentally. An excellent reference on this topic, as well as the theory of random media in general, is the book by Torquato [12].

A key parameter associated with the distribution is the volume fraction, f, of the suspension occupied by the spheres. For very dilute suspensions, the location of the spheres is random with a uniform probability density function. However, as the volume fraction increases, a uniform density function requires some of the spheres to overlap, but since the spheres are assumed to be hard and non-overlapping, the density function must necessarily deviate from a constant. The statistical arrangement of the spheres for any allowable value of f is governed by the so-called pair correlation function, $g_2(\vec{r}_{12})$, where $\vec{r}_{12} = \vec{r}_2 - \vec{r}_1$ is a vector connecting the centers of any two spheres (denoted as particles 1 and 2, located at $\vec{r}_1$ and $\vec{r}_2$, respectively). The underlying assumptions here are: (1) the medium is homogeneous, or spatially stationary, in three-dimensional space, and (2) the potential energy associated with the particle arrangement is dominated by a sum of two-body potential terms, with three-body and higher-order potential contributions being negligible in comparison. For a hard-sphere potential, with identical spheres having radius R, the pair correlation function must be zero for $|\vec{r}_{12}| \leq 2R$. The form of g_2 for separations beyond $2R$ is related to the way in which neighboring spheres are statistically positioned about a central sphere. For large separations in disordered systems with no long-range order, $g_2(r \to \infty)$ asymptotically approaches unity since there is a uniform probability of finding another sphere center in a differential volume element $d\vec{r}$ at any given large separation value.

For a statistically isotropic configuration, we are free to place the coordinate system origin at the center of sphere 1, so $g_2(r)$ then becomes a function of the radial separation $r = |\vec{r}_2|$. In this case, $g_2(r)$ is known as the *radial distribution function*. We note that g_2 is a statistical function that is generally referred to as either a correlation function or a distribution function, but it is instructive to realize that g_2 is fundamentally a type of probability density function. More specifically, if

the average number density of spheres is denoted $\rho = N/V$ (with N being the total number of spheres and V the sample volume), then $\rho g_2(r)\, d\vec{r} = \rho g_2(r) 4\pi r^2 dr$ is the expected number of neighboring sphere centers located within a thin spherical shell of thickness dr at a distance r from the central sphere origin.

It is convenient to define the *total correlation function* $h(\vec{r})$ as

$$h(\vec{r}) = g_2(\vec{r}) - 1. \tag{S26}$$

For disordered systems, $h(\vec{r}) \to 0$ as $r \to \infty$. As noted in most any textbook on statistical mechanics, Ornstein and Zernike in 1914 proposed a decomposition of $h(\vec{r}_{12})$ into a direct part, $c(\vec{r}_{12})$, plus an indirect part given in the form of a superposition integral [13, 14]:

$$\begin{aligned} h(\vec{r}_{12}) &= c(\vec{r}_{12}) + \rho \iiint h(\vec{r}_{23}) c(\vec{r}_{13}) d\vec{r}_3 \\ &= c(\vec{r}_{12}) + \rho \iiint h(\vec{r}_{13} - \vec{r}_{12}) c(\vec{r}_{13}) d\vec{r}_3, \end{aligned} \tag{S27}$$

where $\vec{r}_{ij} = \vec{r}_j - \vec{r}_i$. The direct term accounts for the influence of a particle at $\vec{r}_1$ on one at $\vec{r}_2$, which is generally short-ranged. The indirect part, given by the integral term above, accounts for the influence of a particle at $\vec{r}_1$ on another particle at $\vec{r}_3$, which in turn affects the location of the particle at $\vec{r}_2$ either directly, or indirectly through interaction with other particles. We can simplify the notation by letting $\vec{r} = \vec{r}_{12}$ and $\vec{r}' = \vec{r}_{13}$. Also, for a homogeneous and isotropic system (e.g. monodisperse microspheres), $h(\vec{r}) = h(r)$ and $c(\vec{r}) = c(r)$ are radially symmetric functions of $r = |\vec{r}|$, so the Ornstein-Zernike equation can be written as

$$\begin{aligned} h(r) &= c(r) + \rho \iiint h(|\vec{r} - \vec{r}'|) c(r') d\vec{r}' \\ &= c(r) + \rho \left[h(r) * c(r) \right], \end{aligned} \tag{S28}$$

where the asterik denotes a three-dimensional convolution (not to be confused with a one-dimensional convolution in the radial variable alone; see [15], Sec. 9). In order to solve for both $h(r)$ and $c(r)$, an additional constraint, known as a closure relation, is required. For spheres of radius R, a common approach is to employ the Percus-Yevick (PY) closure approximation which, as noted by Torquato, requires $h(r) = -1$ for $0 \le r \le 2R$, and $c(r) = 0$ for $r > 2R$. Enforcing these boundary conditions leads to an analytical solution for $c(r)$ [16],

$$c(r) = \begin{cases} -\lambda_1 - 3\eta\lambda_2 \left(\dfrac{r}{R}\right) - \dfrac{\eta\lambda_1}{16} \left(\dfrac{r}{R}\right)^3, & r \le 2R \\ 0 & r > 2R, \end{cases} \tag{S29}$$

where

$$\lambda_1 = \frac{(1+2\eta)^2}{(1-\eta)^4}, \qquad \lambda_2 = \frac{(1+\eta/2)^2}{(1-\eta)^4}, \tag{S30}$$

and $\eta = 4\pi\rho R^3/3$. This expression for $c(r)$ can in turn be Fourier transformed to yield (see [12], Eq. 3.61),

$$\begin{aligned} \tilde{c}(s) = \frac{-4\pi}{s^3} \Bigg\{ \lambda_1 \left[\sin q - q\cos q\right] + \frac{6\eta\lambda_2}{q} \left[2q\sin q + (2-q^2)\cos q - 2\right] + \\ \frac{\eta\lambda_1}{2q^3} \left[(4q^3 - 24q)\sin q - (q^4 - 12q^2 + 24)\cos q + 24\right] \Bigg\} \end{aligned} \tag{S31}$$

where $q = 2Rs$ is a dimensionless wave number, and the tilde denotes a Fourier-domain function.

Taking the Fourier transform the Ornstein-Zernike equation (Eq. S28) yields,

$$\tilde{h}(s) = \tilde{c}(s) + \rho\tilde{c}(s)\tilde{h}(s) = \frac{\tilde{c}(s)}{1 - \rho\tilde{c}(s)}. \tag{S32}$$

Applying an inverse transform, we then have

$$h(r) = \mathcal{F}_{3D}^{-1}\left\{\tilde{h}(s)\right\} = \frac{1}{2\pi^2 r} \int_0^\infty \frac{\tilde{c}(s)}{1 - \rho\tilde{c}(s)}\, s\sin(sr) ds. \tag{S33}$$

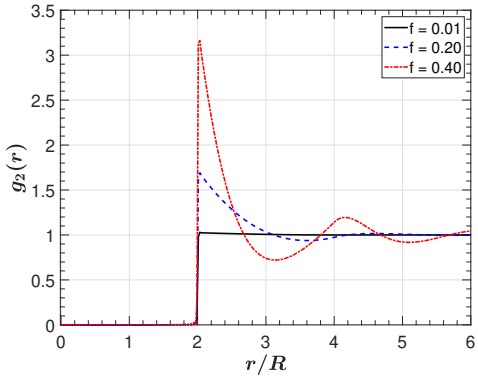

Fig. S3. Plots of the radial distribution function, $g_2(r)$, for a collection of monodisperse microspheres (radius = R) using three different values of normalized concentration, or volume fraction, f = 0.01, 0.20 and 0.40.

It is a reasonably staightforward matter to numerically evaluate this equation for $h(r)$ by using Eq. S31 for $\tilde{c}(s)$, combined with a judiuous choice of sampling in both the spatial and spatial-frequency domains as described by Lado [17]. The radial distribution function, $g_2(r)$, then follows trivially since $g_2(r) = h(r) + 1$. To make the dependence of f explicit in Eq. S33, we note that the average number density of microspheres, $\rho = N/V$, can be expressed in terms of the microsphere volume fraction $f = NV_s/V$ (with V_s being the volume of an individual sphere), so $\rho = f/V_s$. Plots of $g_2(r)$ are shown in Fig. S3 for $f = 0.01$, 0.20 and 0.40.

Our primary interest lies in finding the statistical autocorrelation function for the ensemble of microspheres. The ensemble consists of two phases, with phase 1 being the matrix material surrounding the spheres (e.g., liquid or air) and phase 2 being the spherical particles themselves (e.g., glass or plastic). Following Torquato, we first evaluate the two-point probability function for the spherical-particle phase ([10], Eq. 5.40):

$$\begin{aligned} S_2^{(2)}(r) &= \rho\, m(r) * m(r) + \rho^2 g_2(r) * m(r) * m(r) \\ &= \rho\, m(r) * m(r) + \rho^2 [1 + h(r)] * m(r) * m(r) \\ &= \rho\, m(r) * m(r) + \rho^2 [1 * m(r) * m(r)] + \rho^2 [h(r) * m(r) * m(r)], \end{aligned} \tag{S34}$$

where $m(r)$ is the so-called *indicator function* for a sphere of radius R, expressed in terms of the Heaviside step function as

$$m(r) = H(R - r) = \begin{cases} 1, & r \le R \\ 0, & r > R. \end{cases} \tag{S35}$$

As before, the asterisks in Eq. S34 denote three-dimensional convolutions. This result applies to a statistically homogeneous and isotropic ensemble of impenetrable spheres.

By definition, $S_2^{(2)}(r)$ corresponds to the probability that any two points separated by a distance r are both contained inside spherical particles (the superscript (2) indicates phase 2). The complement, $S_2^{(1)}(r) = S_2^{(2)}(r) + 1 - 2f$, is the probability that the two points reside in the matrix phase. A third option, namely the probability that the first point lies in the matrix and the second point lies in a sphere, is given by $S_2^{(12)}(r) = f - S_2^{(2)}(r)$, with its complement $S_2^{(21)}(r) = S_2^{(12)}(r)$. The sum of all four two-point probability functions therefore equals one. While Torquato refers to $S_n^{(i)}$ as the n-point probability function for phase i, they are mathematically equivalent to n-point correlation functions ([10], Eq. 2.6). Therefore the autocorrelation function of the microsphere ensemble that we seek is

$$\Gamma_e(r) = S_2^{(2)}(r). \tag{S36}$$

To evaluate this function, we return to Eq. S34 and note that

$$m(r) * m(r) = A(r), \tag{S37}$$

where $A(r)$ is the autocorrelation function for an individual sphere (Eq. 66) and, for any constant a,

$$a * m(r) = a \iiint m(r) d\vec{r} = aV_s, \tag{S38}$$

where V_s is the volume of a sphere. Therefore, $1 * m(r) * m(r) = V_s * m(r) = V_s^2$. Combining results, Eq. S36 becomes

$$\Gamma_e(r) = \rho A(r) + \rho^2 V_s^2 + \rho^2 \left[h(r) * A(r) \right]. \tag{S39}$$

It is instructive to consider the value of $\Gamma_e(r)$ in the two limits of $r = 0$ and $r >> 2R$. To do so, we first rewrite Eq. S39 using $\rho = f/V_s$ and $h(r) = g_2(r) - 1$, obtaining

$$\Gamma_e(r) = \frac{f}{V_s} A(r) + f^2 + \left(\frac{f}{V_s} \right)^2 \left\{ \left[g_2(r) * A(r) \right] - \left[1 * A(r) \right] \right\}. \tag{S40}$$

For $r = 0$ we know $A_s(0) = V_s$. Also we observe that $[g_2(r) * A(r)](0) = 0$. In other words, the overlap integral of $g_2(r)$ times $A(r)$ at zero shift must be identically zero because $g_2(r) = 0$ for $0 \leq r \leq 2R$, while $A(r)$ is zero for $r \geq 2R$. Finally, we have $[1 * A(r)](0) = V_s^2$ because the volume integral of $A(r)$ over 3D space is V_s^2. Putting these findings together leads to the following simple result

$$\Gamma_e(0) = f. \tag{S41}$$

Thus we see the normalized autocorrelation function of the microsphere ensemble is

$$\gamma_e(r) = \frac{\Gamma_e(r)}{\Gamma_e(0)} = \frac{\Gamma_e(r)}{f}. \tag{S42}$$

For the case of $r >> 2R$, we have $A_s = 0$ and $g_2 \to 1$. This last relation means that for a large shift, the convolution $[g_2(r) * A(r)] \to [1 * A(r)]$. We are therefore left with

$$\Gamma_e(r >> 2R) = f^2. \tag{S43}$$

From this result it follows that the large-r limit of $\gamma_e(r)$ has an asymptote equal to f. Assuming the particle distribution is spatially ergodic, $\gamma_e(r)$ corresponds to the normalized overlap volume of a random distribution of spheres with a copy of the distribution shifted in any direction by r. A non-zero asymptote means there remains a constant overlap volume for arbitrarily large shifts.

For purposes of numerical computation, we again return to Eq. S34 and note that the last term is preferably evaluated in the Fourier domain, thereby converting the following more tedious double spatial convolution into the inverse transform of a product,

$$h(r) * m(r) * m(r) = \mathcal{F}_{3D}^{-1} \left\{ \tilde{h}(s) \tilde{m}^2(s) \right\}, \tag{S44}$$

where

$$\tilde{m}(s) = \frac{4\pi}{s} \int_0^R r \sin(sr) dr = \frac{4\pi}{s} \left[\frac{\sin(sR)}{s^2} - \frac{R\cos(sR)}{s} \right]. \tag{S45}$$

Using these Fourier domain results, Eq. S39 becomes,

$$\Gamma_e(r) = \rho A(r) + \rho^2 V_s^2 + \rho^2 \mathcal{F}_{3D}^{-1} \left\{ \tilde{h}(s) \tilde{m}^2(s) \right\}. \tag{S46}$$

Finally, to again make the dependence on f explicit, we substitute $\rho = N/V = f/V_s$ (recall ρ is the average number density of spheres) and arrive at following alternative expression for the normalized ensemble autocorrelation function,

$$\gamma_e(r) = \frac{A(r)}{V_s} + f \left[1 + \frac{1}{V_s^2} \mathcal{F}_{3D}^{-1} \left\{ \tilde{h}(s) \tilde{m}^2(s) \right\} \right]. \tag{S47}$$

As with Eq. S33, the inverse Fourier transform in the last term of this equation can be quite easily evaluated numerically via a sum with proper sampling. For very dilute suspensions, as $f \to 0$, we see that $\gamma_e(r) \to A(r)/V_s$, meaning the ensemble autocorrelation function asymptotically approaches the normalized autocorrelation function of a single sphere. In Figure S4(a), we plot $\gamma_e(r)$ for three different values of f.

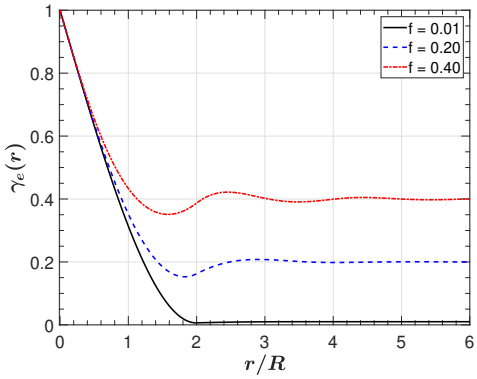

Fig. S4. Normalized 3D autocorrelation functions for a collection of monodisperse hard microspheres (radius = R) using three different values of normalized concentration, or volume fraction, f = 0.01, 0.20 and 0.40, calculated using the PY approximation to the Ornstein-Zernike equation.

REFERENCES

1. Z.-T. Wang, K.-J. Kang, Z.-F. Huang, and Z.-Q. Chen, "Quantitative grating-based x-ray dark-field computed tomography," Appl. Phys. Lett. **95**, 094105 (2009).
2. M. Bech, O. Bunk, T. Donath, R. Feidenhans'l, C. David, and F. Pfeiffer, "Quantitative x-ray dark-field computed tomography," Phys. Medicine Biol. **55**, 5529–5539 (2010).
3. M. Strobl, "General solution for quantitative dark-field contrast imaging with grating interferometers," Sci. Reports **4**, 7243 (2014).
4. J. Graetz, A. Balles, R. Hanke, and S. Zabler, "Review and experimental verification of x-ray dark-field signal interpretations with respect to quantitative isotropic and anisotropic dark-field computed tomography," Phys. Medicine & Biol. **65**, 235017 (2020).
5. J. W. Goodman, *Speckle Phenomena in Optics: Theory and Applications* (SPIE, 2020), 2nd ed.
6. T. Donath, M. Chabior, F. Pfeiffer, O. Bunk, E. Reznikova, J. Mohr, E. Hempel, S. Popescu, M. Hoheisel, M. Schuster, J. Baumann, and C. David, "Inverse geometry for grating-based x-ray phase-contrast imaging," J. Appl. Phys. **106**, 054703 (2009).
7. T. Weitkamp, C. David, C. Kottler, O. Bunk, and F. Pfeiffer, "Tomography with grating interferometers at low-brilliance sources," in *Developments in X-Ray Tomography V*, vol. 6318 U. Bonse, ed., International Society for Optics and Photonics (SPIE, 2006), pp. 249 – 258.
8. J. Mertz, *Introduction to Optical Microscopy* (Roberts & Company, 2010).
9. D. Zwillinger, ed., *CRC Standard Mathematical Tables and Formulae* (Chapman & Hall / CRC, 2003).
10. S. Torquato and G. Stell, "Microstructure of two-phase random media. V. The n-point matrix probability functions for impenetrable spheres," The J. Chem. Phys. **82**, 980–987 (1985).
11. S. H. Lee, S. M. Han, and S. E. Han, "Characterizing randomness in photonic glasses using autocorrelation functions of two-dimensional images," Opt. Express **27**, 35842–35855 (2019).
12. S. Torquato, *Random Heterogeneous Materials, Microstructure and Macroscopic Properties* (Springer, 2002).
13. R. E. Wilde and S. Singh, *Statistical Mechanics, Fundamentals and Modern Applications* (Wiley, 1997).
14. L. S. Ornstein and F. Zernike, "Accidental deviations of density and opalescence at the critical point of a single substance," Proc. Royal Neth. Acad. Arts Sci. **17**, 793 – 806 (1914).
15. N. Baddour, "Operational and convolution properties of two-dimensional Fourier transforms in polar coordinates," J. Opt. Soc. Am. A **26**, 1767–1777 (2009).
16. M. S. Wertheim, "Exact solution of the Percus-Yevick integral equation for hard spheres," Phys. Rev. Lett. **10**, 321–323 (1963).
17. F. Lado, "Numerical Fourier transforms in one, two, and three dimensions for liquid state calculations," J. Comput. Phys. **8**, 417–433 (1971).